# Human cortical areas are sparsely connected: Combining histology with diffusion MRI to estimate the absolute number of axons

**Burke Q. Rosen[1*], Eric Halgren[1,2]**

[1]Neurosciences Graduate Program, University of California, San Diego, La Jolla CA 92093
[2]Depts. of Neurosciences & Radiology, University of California, San Diego, La Jolla CA 92093

[*]bqrosen@health.ucsd.edu
3510 Dunhill St.
San Diego, CA 92101
858-405-9660

**Short Title**:
Human cortical areas are sparsely connected

**Author Roles**:
E.H. : conceptualization, supervision, funding acquisition, writing – original draft preparation, writing review & editing
B.Q.R. : investigation, formal analysis, data curation, methodology, software, visualization, writing – original draft preparation, writing review & editing

**Competing Interest Statement**:
The authors declare no competing interests.

**Keywords**:
diffusion MRI | structural connectivity | white matter | neuroanatomy | Human Connectome Project

**Preprint Servers**:
A version of this article was deposited in bioRxiv, https://doi.org/10.1101/2021.06.07.447453.

**Abstract** The tracts between cortical areas are conceived as playing a central role in cortical information processing, but their actual numbers have never been determined in humans. Here we estimate the absolute number of axons linking cortical areas from a whole-cortex diffusion-MRI (dMRI) connectome, calibrated using the histologically-measured callosal fiber density. Median connectivity is estimated as ~6200 axons between cortical areas within-hemisphere and ~1300 axons inter-hemispherically, with axons connecting functionally-related areas surprisingly sparse. For example, we estimate that <5% of the axons in the trunk of the arcuate and superior longitudinal fasciculi connect Wernicke's and Broca's areas. These results suggest that detailed information is transmitted between cortical areas either via linkage of the dense local connections or via rare, extraordinarily privileged long-range connections.

## Introduction

The major tracts connecting cortical areas have long been central to models of information-processing in the human brain [1]. Such models have been refined and applied to development and disease with the advent of diffusion-MRI or dMRI [2]. However, dMRI only provides *relative* connectivity, not the absolute number of axons. Relative connectivity is very useful in many circumstances but more constraints would be possible if the absolute number of axons connecting different cortical areas could be estimated. Here we describe and apply a novel method for translating from dMRI-derived streamlines to axon counts.

The ratio between these two measures is obtained by comparing the number of streamlines pass through the corpus callosum to the number of axons, as measured with histology. The corpus callosum is uniquely well-suited for this purpose. Electron microscopy (EM) can be used to unambiguously count the total number of callosal axons because the limits of the callosum are well-defined, axons are aligned, and sections can be cut perpendicular to their axis. Likewise, dMRI-derived streamlines can be

unambiguously and exhaustively assigned to the callosum because the source and destination of all axons passing through the callosum as a whole are well-defined. In contrast to the ipsilateral fiber tracts, in which the majority of axons enter or leave the tract at point between the fascicular terminals, commissural axons must all be connecting the two hemispheres. Fortunately, despite these differences, the mean and variability of cross-sectional axon density of the corpus callosum is quite similar to that of telencephalic white matter in general [3–5], permitting the streamline:axon ratio calculated from callosal fiber to be applied to intra-hemispheric connections.

It has long been recognized that as the number of cortical neurons increases, maintaining the same probability of connectivity between neurons would require that axon number increase approximately with the square of neuron number, and this would require too much volume, impose an unsustainable metabolic load [6], and actually decrease computational power due to conduction delays [7]. The consequent imperative to minimize long distance cortico-cortical fibers has been posited to be reflected in exponential decline in cortical connectivity with distance [8], and to be partially compensated for with a small-world graph architecture [9], granting special properties to rare long-distance fibers in a log-normal neural physiology and anatomy [10]. However, this organizing principle is rarely explicitly addressed in terms of individual axon counts, nor in a manner both granular and exhaustive with respect to cortical areas. In our histologically calibrated dMRI-derived estimation of this intercortical axon counts, we find that the widespread cortical integration implied by behavioral and mental coherence, and routinely observed in widespread physiological synchronization, belies a surprising small absolute number of long-range axons connecting cortical areas.

## Materials and Methods

The basic principle of our method is very simple. Given a dMRI-based measure of total inter-hemispheric connectivity in arbitrary units and the physical number of axons traversing the corpus

100 callosum, the conversion factor between the two can be obtained by dividing the first by the second.
101 Specifically, we started with the total inter-hemispheric tractography strength reported in our dMRI
102 connectome of the Human Connectome Project (HCP) cohort [11]. For each individual, the cross-
103 sectional area of the corpus callosum was obtained using the standard FreeSurfer structural MRI
104 pipeline [12]. Multiplying this number by a histologically ascertained callosal fiber density [3] yields an
105 estimate of the number of axons traversing an individual's corpus callosum. Dividing this count by
106 individuals' inter-hemispheric dMRI streamline value yields the conversion ratio from the arbitrarily-
107 scaled dMRI metric to the absolute number of axons. Note that this procedure is independent from the
108 scale of the dMRI metric, requiring only that it be proportional to the absolute number of fibers. A
109 moderate proportionality has been observed in a comparison of dMRI and retrograde tracing in
110 macaques [13,14]. Therefore, while the ratio itself is study-specific, the procedure can be applied to
111 any dMRI tractography method or parameter set, provided that the dMRI method returns a continuous
112 distribution of connectivity values and has reasonably similar sensitivity to callosal and ipsilateral fiber
113 tracts. To demonstrate this, we repeated the analysis using data from an alternate tractography of the
114 HCP cohort [15]. For detailed methodology, see S1 Appendix: Extended Methods and Results.

115 **Results**

116 Our previous dMRI study [11] includes estimated tractography streamlines between all 360 parcels of
117 the HCP-MMP1.0 atlas [16] for each of the 1,065 individuals in the HCP dMRI cohort. The sum
118 connectivity between the 180 left hemisphere cortical parcels and the 180 right ($180^2$ parcel pairs)
119 constitutes the total callosal connectivity, on average $1.25 \times 10^8$ streamlines. Based on our assumed
120 fiber density of $3.7 \times 10^5$ axons/mm$^2$ [3] and measured callosal cross-sectional area (mean =
121 689.45mm$^2$), we estimate this cohort to have $2.6 \times 10^8$ callosal fibers on average. The mean quotient

122 between these two quantities is 2.00 axons-per-streamline, a ratio specific to the dMRI methodology
123 and parameters used.
124 Applying the conversion factor to the inter-parcel connectivity from our prior study yields an
125 estimate of the absolute number of axons connecting different cortical areas (Fig 1A), $2.43 \times 10^9$ axons
126 in total. This implies that <22% of the ~$11.5 \times 10^9$ cortical pyramidal cells [17,18] project outside their
127 parcel with the remainder being short-range horizontal or U-fibers. Furthermore, because 51% of inter-
128 areal axons are to adjacent areas, <11% of pyramidal cells project beyond the adjacent parcel. Axons
129 are approximately log-normally distributed among non-adjacent parcel pairs, with adjacent pairs
130 having disproportionally high axon counts (Fig 1B). Median connectivity is ~6,200 axons between
131 cortical areas in the same hemisphere, and ~1,300 inter-hemispherically. The number of axons in the
132 median *inter*-hemispheric connection is ~20% of that in the median *intra*-hemispheric connection,
133 similar to that found with histological tracing in macaques [19]. The number of callosal axons is not
134 significantly affected by subject sex, though subjects ages 26-30 have slightly more inter-hemispheric
135 axons than subjects ages 22-15 (S3 Fig). This sparse long-range connectivity is consistent with its
136 exponential fall-off measured with dMRI in humans and histologically in other mammals [8,11] and with
137 previous statistical estimates based on traditional neuroanatomy [20]. In comparison to the number of
138 axons that would be necessary for complete interconnectivity of neurons in different cortical areas with
139 each other, the estimated number is ~$10^{11}$ times smaller (see S1 Appendix for calculation).
140 Our method requires that dMRI-tractography performs in a roughly similar manner when applied to
141 intra- versus inter-hemispheric connections. We evaluated this similarity by comparing linear
142 regressions of distance-matched log-transformed streamlines, and found no difference between the
143 slope or intercept of inter- and intra-hemispheric connections (Fig 1C); within the common distance
144 domain a paired r-test showed no difference in correlation, $p = 0.58$. The total count of a parcel's

145 axons to or from all other areas is much less variable when normalized by the parcel's area (Fig 1D,E).
146 Multiplying the total number of fibers by the effective fiber cross-sectional area (the inverse callosal
147 packing density, $2.7 \times 10^{-6}$ $mm^2$/axon) yields $6.6 \times 10^3$ $mm^2$ of cortex or 3.7% of the total white-gray
148 interface. Note that the effective axonal area includes myelin, supporting cells and intercellular space
149 in addition to the axon proper. The cross-sectional packing density of human prefrontal white matter is
150 quite similar to callosal values with an average of $3.5 \times 10^5$ myelinated axons/$mm^2$ [4] after correction for
151 tissue shrinkage, and this varies among prefrontal regions by a less than factor of 2 [5]. The percent of
152 fiber-allocated cortical area is quite similar to the ~4% of total cortical fibers Schüz and Braitenberg
153 estimated [20] are contained in the corpus callosum and long fascicles. The remaining ~95% of the
154 cortical gray-white interface area is likely occupied by the short range U-fiber system which is difficult
155 to assess with dMRI.

156 We estimated the fraction of axons traversing the entire length of the arcuate / superior lateral
157 fasciculus (AF/SLF) between termination fields centered on Broca's and Wernicke's areas. The total
158 number of AF/SLF axons was derived by multiplying the tracts' cross-sectional areas by mean axon
159 density of ipsilateral tracts. Using published estimates of the cross-sectional areas of 160.6 $mm^2$ and
160 51.5 $mm^2$ for the left and right AF and 213.8 $mm^2$ and 174.4 for the left and right SLF [21], and a
161 shrinkage-corrected axon density of $3.5 \times 10^5$ axons/$mm^2$ [4], yields a total of $1.3 \times 10^8$ and $0.8 \times 10^8$ axons
162 in the left and right AF/SLF. These values were compared to the number of tractography-derived axons
163 connecting AF/SLF termination fields [16] according to consensus definitions from reference [22], see
164 S4 Fig. When the anterior termination field, centered on Broca's area is defined as HCP-MMP1.0
165 parcels 44, 45, 6r, IFSa, IFSp, and FOP4 and the posterior termination field, centered on Wernicke's
166 area as parcels PSL, RI, STV, and PFcm, trans-terminal axons account for only 0.6% and 0.8% of tract
167 axons in the left and right hemispheres. If the termination fields are liberally expanded to also include

168 parcels 47l and p47r in Broca's and parcels PF, PFm, and PGi in Wernicke's then these percentages
169 increase to a still modest 1.9% and 2.9% of total tract axons. Please note that in this calculation all
170 axons between Broca's and Wernicke's areas are assumed to pass through the AF/SLF; to the degree
171 that some pass outside the AF/SLF, our estimates should be decreased.

172 The volume of hemispheric white matter (WM) occupied by axons between cortical parcels is equal
173 to the sum of all axons' lengths multiplied by their cross-sectional areas. The mean fiber tract lengths of
174 connections were taken from our prior dMRI analysis [11]. For the effective cross-sectional area of
175 axons we again assumed an effective cross-sectional area equivalent to the inverse of the callosal fiber
176 density [3]. So calculated, the volume occupied by cortico-cortical and hippocampo-cortical fibers is
177 $4.3 \times 10^5$ $mm^3$, or about 96% of the total MRI-assessed WM volume. This implies that the number of
178 long-range fibers cannot be larger than our estimate unless the axon density calculated from the
179 corpus callosum histology is mistakenly low, but this is a linear effect that would need to be
180 unrealistically inaccurate for it to change our main conclusions. Another possibility is that axon density
181 was correctly measured for the corpus callosum but is higher for intra-hemispheric fibers *and* the
182 number of axons per streamline is higher intra- than inter-hemispherically. These both need to be the
183 case because there is no space available in the hemispheric white matter to contain more axons unless
184 they are smaller. However, the histological data indicates that axonal density is approximately the
185 same intra- and inter-hemispherically [3,4] and the comparison of distance-matched streamlines (Fig.
186 1*C*). suggests that the number of axons per streamline intra- and inter-hemispherically is also
187 approximately equal. The remaining WM volume may seem insufficient for connections with
188 subcortical structures. However, the major subcortical structures known to communicate with the
189 cortex (thalamus, amygdala, striatum, nucleus basalis, locus coeruleus, etc.) contain, in sum, less than
190 1% of the number of cortical neurons [23–25], see S1 Appendix: Extended Methods and Results. Even

191 under the unlikely assumption that all excitatory thalamic neurons project to the cortex with a density
192 across all cortical parcels proportionally to their area, their axons would only comprise ~4% of the total
193 WM volume.

194 We conducted a series of simulations examining the consequences of possible errors in axonal
195 packing density and axon-to-streamline ratio. As noted above, these parameters are co-constrained by
196 the physical volume available for white matter. At our derived ratio and assumed packing density, the
197 volume of inter-areal axons is just under the observed total white matter volume. Large net errors in
198 the assumed packing density would result in total inter-areal axon volumes that are inconsistent with
199 the hemispheric white matter volume, a value that is well established. Consequently, in our
200 simulations, axonal packing density and axon-to-streamline ratio were reciprocally changed in order to
201 maintain a constant total cerebral white matter volume. Since our parameter estimates are based
202 primarily on fibers passing through the callosum, which are longer in general than intra-hemispheric
203 fibers, parameter inaccuracies are more likely for short fibers. In order to evaluate the effect of such
204 inaccuracies, we first simulated the effect of assuming that dMRI sensitivity is systematically reduced
205 (and thus axon count underestimated) for shorter fibers. Uniformly doubling the number of axons with
206 lengths < 40 mm in this way yields only a 37.5% increase in the total number of inter-areal axons, and
207 because rank-order of observations is not altered the median axon counts are unchanged.
208 Conceivably, our parameter estimates are accurate for the longest fibers (which tend to pass through
209 the callosum) but are progressively less accurate for shorter inter-areal distances. Consequently, we
210 simulated assuming that our packing density and dMRI sensitivity estimates at the longest fiber lengths
211 were as in our base model, and then increased the dMRI streamline-to-axon ratio linearly as the fibers
212 got shorter. Axon density was adjusted to maintain white matter volume constant. Even with
213 unrealistically large systematic and matched errors in the two estimates, median inter-areal axon count

214 are only modestly increased, see S5 Fig. For example, adjustments resulting in twice the axon density
215 and half the sensitivity of dMRI to axons at short inter-parcel distances increase the median number of
216 inter-parcel axons by only ~36%. As reviewed below, errors in inter-areal axon count due to miss-
217 estimation of axonal packing density are likely to be relatively unbiased with respect to inter-areal fiber
218 length, and reported measures vary less than a factor of two. Our simulations indicate that such errors
219 would have only marginal effects on the median number of inter-areal axons.

220 In order to demonstrate that the key principles and findings of this report are robust to the details
221 of tractography procedure, we repeated our analysis on the tractography data of Arnatkeviciute and
222 colleagues [15]. These data consist of a 972 subject subset of the HCP cohort and use the same
223 parcellation but a different method to reconstruct the fiber streamlines. These data contain fewer
224 streamlines and the estimated numbers of axons per connection are broadly comparable, being
225 somewhat fewer but within an order of magnitude of our primary estimate. We find $8.4 \times 10^8$ total axons
226 and $1.1 \times 10^8$ callosal axons per subject on average, with medians of ~1100 and ~130 axons for pairwise
227 intra- and inter-hemispheric connections between cortical areas (S2 Fig), i.e., even more sparse than
228 those calculated from our tractography data. These data confirm that, independent of tractography
229 procedure, cortical areas are sparsely connected.

230

231 **Discussion**

232 In this study we estimated the absolute number of axons interconnecting cortical areas by calibrating
233 dMRI-based tractography using the histologically ascertained cross-sectional fiber density of the
234 corpus callosum and found that long-range cortico-cortical connections are quite sparse. Our method
235 depends on histological estimates of callosal axon packing density and leverages the unique
236 properties of the callosum. It assumes proportionality between the number of axons connecting two

237 areas and the number of dMRI tractography streamlines for the areal pair, and it assumes approximate
238 parity between dMRI sensitivity to inter- and intra-hemispheric connections. In order to estimate the
239 volume occupied by inter-parcel cortico-cortical connections, we make the further assumption that the
240 effective axonal packing density is reasonably uniform across the hemispheric white matter.

241 Although there are few reports of axonal density in the corpus callosum [3,26], they are consistent
242 with each other and with reports of axonal density of intra-hemispheric tracts [4]. Our study relies on
243 the data reported by Aboitiz et al. [3], because it is the most systematic count of which we are aware.
244 There is a later study, [26], which provides a value only slightly lower, $2.83 \times 10^5$ vs $3.7 \times 10^5$ axons/mm$^2$
245 after correction for tissue shrinkage [27]. However, since this later study was primarily a survey of axon
246 diameter with packing density only incidentally recorded, it is conceivable that density values derived
247 from could be small underestimates. Mis-estimated tissue shrinkage is possible but likely to be <10%
248 and callosal areas were measured with a well-validated and widely-used in vivo method [12]. The axon
249 count estimate does not require that the packing densities of the corpus callosum and ipsilateral white
250 matter be the same, but rather the lesser assumption that the axon to dMRI streamline ratio be
251 reasonably uniform across the various instances of long distance cortico-cortical connectivity.
252 However, if the packing densities of ipsilateral and callosal long distance connections are also similar
253 then the total hemispheric white matter volume provides an absolute constraint on the number of long
254 distance connections, and this provides a powerful validation of our estimate.

255 The literature provides converging evidence that the fiber packing density of white matter varies by
256 at most a factor of 2 across the cortex, including the corpus callosum. A histological study of human
257 cortex found only a 7% difference in the axon densities of the callosum versus the superior longitudinal
258 and inferior occipitofrontal fasciculi [26]. Zikopolous and Barbas [4] found that the cross-sectional
259 packing density of human prefrontal white matter is remarkably similar to callosal values with an

260 average of $3.5 \times 10^5$ myelinated axons/$mm^2$ after correction for tissue shrinkage and that this varies
261 among prefrontal regions by a less than factor of 2 [5]. In addition, while dMRI-based estimates of axon
262 density and caliber are imperfect, they suggest that axon density varies by less than 2-fold both
263 between major ipsilateral tracts and within each tract along their length [28]. While packing density is
264 not directly equivalent to axon caliber, the two are likely inversely related. Axon diameter, as estimated
265 with dMRI, varies by 20% among ipsilateral tracts and by at most a factor of 2.2 among white matter
266 voxels, including those of the corpus callosum [29,30]. Overall, distributions of dMRI-derived axon
267 diameter for the callosum [31] and whole cerebrum [30] are similar with the bulk of values between 2.5
268 and 5 μm. Histological measurements in macaques concur that axon diameters are very similar within
269 the callosal and non-callosal segments of major fasciculi and vary by less than 2-fold across the cortex
270 [32]. Furthermore, even this limited variation in diameter is not systematically dependent on the length
271 of axons but rather on their regions of origin and termination [33].
272 Concerning dMRI- to-axon-count proportionality, it has been shown in macaques that there is a
273 moderate linear correlation between dMRI-traced streamlines and the number of fibers identified with
274 histological tracers connecting cortical regions [13,14]. Based on these data, Donahue and colleagues
275 [13] concluded that dMRI tractography was capable of quantitively describing cortico-cortical white
276 matter tracts with approximately order-of-magnitude precision using a high-quality dataset such as the
277 HCP. In line with previous statistical estimates of whole-cortex axon counts based on traditional
278 neuroanatomy [20], the numbers of axons in pairwise connections are probably correct within an order
279 of magnitude. Estimates of this precision are useful as we find that that inter-areal connectivity derived
280 from dMRI varies over more than seven orders of magnitude.
281 While we derive a single dMRI-to-axon count factor, it is likely that the true conversion ratio varies
282 somewhat among connections due to local microstructural differences other than axon count such as

283 axon caliber, packing density, or myelination. However, the major fasciculi (including the corpus
284 callosum) have similar axon calibers and packing densities, varying by only a factor of ~2 across the
285 cortex when examined in humans histologically [4,5,26] or with dMRI [28–30] and histologically in
286 macaques [32]. More generally, packing density is a function of local cellular interactions, especially
287 with oligodendrocytes, and because these are the same in the corpus callosum and intra-hemispheric
288 white matter, the *a priori* expectation is that packing density would be similar, as histological data
289 supports. Myelination has only a modulatory effect on dMRI-detected anisotropy, with most of the
290 effect derived from axonal membranes [34]. Nevertheless, microstructural variation in dMRI-to-axon
291 count ratio may be a source of noise in our estimates. Our simulations of miss-estimation of dMRI-to-
292 axon ratio and packing density show that these errors only marginally affect estimated axon counts and
293 do not alter our conclusions. Our findings were also similar when we repeated our analysis on an
294 alternative, somewhat sparser dMRI tractography dataset [15], demonstrating that the details of the
295 tractography algorithm do not affect the overall tenor of our results. While the scope of this study is
296 limited to long-range fibers, we note that shorter, more superficial U-fibers are systematically less
297 myelinated and of lesser caliber than their inter-areal counterparts [5] and therefore the procedure
298 outlined here may require modification before being applied to them.
299 As previously stated, this methodology assumes a reasonable degree of parity in the sensitivity of
300 the dMRI tractography to intra- and inter-hemispheric fiber tracts. Consistent with this assumption, we
301 found little difference between distance-matched dMRI connectivity for callosal versus ipsilateral
302 connections. If callosal axons were more easily detectable, this would be reflected as an upward
303 displacement of the inter-hemispheric trace (blue) above the intra-hemispheric trace (green) across the
304 entire distance domain in Fig 1C, which is not evident. This parity is perhaps unsurprising because
305 over most of their trajectories, inter-hemispheric fibers are subjected to the same crossing fiber issues

306 as intra-hemispheric. Specifically, the corpus callosum is a distinct tract for only about 15-35 mm, but
307 its fibers range in length up to about 300 mm. Thus, the fraction of an inter-hemispheric tract that
308 resides within the callosum is inversely proportional to its total length. Consequently, if there were
309 enhanced detection of callosal fibers as streamlines by dMRI, one would expect the inter-hemispheric
310 (blue) trace in Fig 1C to be elevated primarily at short fiber lengths and depressed at long fiber
311 lengths, resulting in a noticeably steeper slope for the inter-hemispheric than the intra-hemispheric
312 trace, which is not observed. These data support the applicability of the scaling factor derived from
313 inter-hemispheric fibers to intra-hemispheric fibers.

314 The corpus callosum was used to calibrate the estimate because of its unique properties: it has a
315 well-defined cross-sectional area, more than ~99% of inter-hemispheric cortico-cortical axons are
316 routed through it [3,35], and essentially no fibers leave or enter the tract between the two
317 hemispheres. This is in sharp contrast to non-commissural fasciculi. While it may be commonly
318 assumed that within major cortical fasciculi the majority of axons terminate or originate at the ends of
319 the tract and thus carry information along its entire length, an alternative conception is that these large
320 bundles are composed mostly of axons shorter than the total fascicular length which enter and exit the
321 tract at various points. By analogy, the former assumption likens a tract to a tunnel, where all traffic is
322 trans-terminal, whereas the latter conceives of tracts as like interstate highways, where very few
323 vehicles travel the entire route. In a supplementary analysis we compared these models for the arcuate
324 / superior lateral fascicular (AF/SLF) system. The total number of AF/SLF axons was estimated using the
325 tract diameters [21] and packing densities [4] taken from the literature. The number of trans-terminal
326 axons was determined by defining termination field parcels centered on restricted and inclusive
327 definitions of Broca's and Wernicke's areas [22]. Depending on the assumptions, only about 1-5% of
328 the axons in a middle section of these fasciculi are trans-terminal. These percentages may be over-

329 estimates since they assume that all fibers between the posterior and anterior areas travel through the
330 AF/SLF. However, even if these values are a 2-fold underestimate, it suggests that only a small fraction
331 of the axons in the ipsilateral fasciculi are trans-terminal. The evidence indicates that the 'highway'
332 model is more apt for the ipsilateral fiber tracts and this conception is consistent with neural wiring
333 being driven, in large part, by exponential distance rules [8]. This of course, does not apply to the
334 corpus callosum, as there is no inter-terminal cortex to project into.

335 Importantly, the reconceptualization of major intra-hemispheric tracts as containing few fibers
336 connecting their distant terminals is still consistent with the long- and well-established impression from
337 blunt dissection [36] and dMRI orientation maps [37] that the hemispheric white matter is largely
338 composed of well-defined long-distance tracts. Indeed, we estimate that ~96% of the white matter is
339 composed of inter-areal axons. What these observations suggest is that the major tracts arise from the
340 tendency of axons to grow in alignment with axons which are already present using established
341 mechanisms of adhesion and fasciculation [38]. Thus axons are free to join tracts at various points, and
342 tend to proceed together (fasciculate), but again are free to leave whenever they approach their own
343 target. In other words, axons are joined in a given tract because they share a direction rather than an
344 origin and destination.

345 The inter-areal axon counts we derive here permit other interesting quantitative estimates which
346 may inform models of cortical neurophysiology. For example, the connections between Wernicke's
347 and Broca's areas are thought to integrate receptive and expressive aspects of language, but we
348 estimate that there are only ~58,000 axons between the core cortical parcels in these regions (parcels
349 44 and PSL), fewer than two for each word in an average university student's vocabulary [39]. Another
350 example where quantitative appreciation of direct axonal connections may influence neuro-cognitive
351 models are the hippocampo-cortical interactions subserving recent memory, which are commonly

352 posited to carry information regarding the contents of the memory trace during memory formation,
353 consolidation and retrieval. We estimated that areas distant from the hippocampus, notably the
354 dorsolateral prefrontal cortex, may be connected to it by <10 axons/mm$^2$ (Fig 1F) including both
355 efferent and afferent axons, yet hippocampo-prefrontal interactions are considered crucial for
356 contextual recall [40]. We estimated the average neural density in the cortex as ~92,300 neurons/mm$^2$
357 by dividing the 16.34x10$^9$ cortical neurons (including interneurons) from [17] by the 1.77x10$^5$ mm$^2$
358 mean white–gray surface area of the HCP cohort used. If the sparse connectivity suggested by our
359 calculations is correct, it implies that hippocampo-dorsolateral prefrontal interactions in memory are
360 likely mediated by polysynaptic pathways.

361 These constraints encourage consideration of models of cortical function where connections are
362 dense but mainly local, i.e. a small world network with intense interconnections within modules and
363 sparse projections between them. While this general principle is widely accepted, the scale of the vast
364 gulf in absolute connectivity between local and long-range connections is startling. This network
365 architecture provides for the wide and efficient distribution of information created by local processing
366 within modules [8,9]. A more uniformly connected cortex would require more white matter,
367 necessitating a more voluminous cerebrum and the human cortex is near the limit after which an
368 increase in size reduces computational power [6,7]. Functionally, a deep reservoir of weak connections
369 enables a large number of states and eases state transitions [10]. Modeling suggests that long range
370 covariance and even synchrony can be achieved through activation of multi-synaptic pathways rather
371 than direct connections [41,42], and possible signs of these have been observed experimentally in
372 humans [43,44].

373 While the long-range direct cortico-cortical axons are few in number, we note that axons are
374 heterogeneous and that these counts are a limited proxy for true inter-areal connectivity. Axons,

375 especially those connecting architectonically similar regions, may have a disproportionate impact on
376 the flow of information despite their rarity [45–47], by virtue of their morphology (e.g. greater
377 diameter, larger termination fields, greater axonal arborization, or more numerous *en passant*
378 varicosities) or by molecular synaptic specializations. For example, while only ~5% of the synapses to
379 V1 layer 4 come from the lateral geniculate body in the macaque [48], they have an outsized effect on
380 their firing [49]. The importance of rare inter-module connections might also be enhanced if they are
381 focused on a small location within cortical parcels (i.e. the rich club [50]), but this has not been
382 convincingly demonstrated. Lastly, it is useful to note that these quantitative considerations are
383 radically different in other species, where the smaller number of cortical neurons and shorter inter-
384 areal distances allow greater connectivity between cortical areas, as well as a larger proportion of
385 subcortical connectivity [7].
386

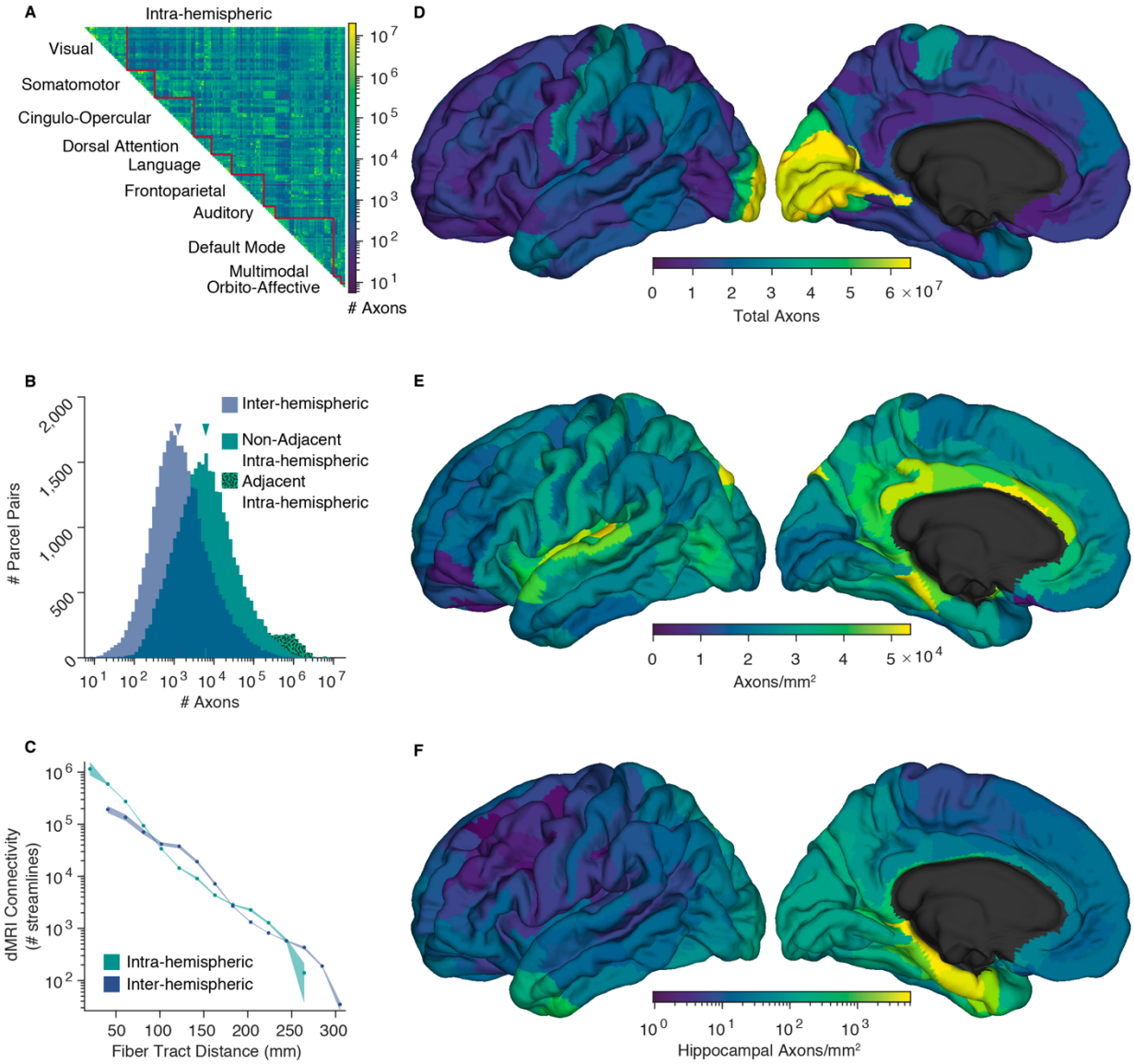


**Fig 1.** The number of axons estimated to interconnect the 360 cortical parcels of the HCP-MMP1.0 atlas. **(A)** Connectivity matrix of intra-hemispheric axon counts, averaged across the two hemispheres. Parcels are ordered into 10 functional networks. **(B)** Histograms showing the distribution of inter- and intra-hemispheric pairwise axon counts. Physically adjacent and non-adjacent parcel pair intra-hemispheric histograms are stacked. Median connectivity, indicated, is ~6,200 axons between cortical areas in the same hemisphere, and ~1,300 inter-hemispherically. **(C)** Comparison of intra- and inter-hemispheric dMRI connectivity as a function fiber tract distance. Pairwise values averaged within 15

fiber-length bins. Shading shows bootstrapped 95% confidence intervals. **(D-F)** axon counts and densities averaged across the two hemispheres and visualized on the left fsaverage template cortex [12]. **(D)** total axons connecting each parcel to all others. **(E)** axons connecting each parcel to all others, normalized by the reference parcel's area. **(F)** axons connecting the hippocampus to the rest of the cortex, normalized by the area of the cortical parcel, shown in log scale.

## Acknowledgements

This work was supported by National Institutes of Health grants RF1MH117155 and R01NS109553 (EH). Data were provided, in part, by the Human Connectome Project, WU-Minn Consortium (Principal Investigators: David Van Essen and Kamil Ugurbil; 1U54MH091657) funded by the 16 National Institutes of Health (NIH) Institutes and Centers that support the NIH Blueprint for Neuroscience Research; and by the McDonnell Center for Systems Neuroscience at Washington University. The funders had no role in study design, data collection and analysis, decision to publish, or preparation of the manuscript.

## Data availability

The processed data used in this study are available at https://doi.org/10.5281/zenodo.5912108. Datafiles are in Matlab v7.3 format. The Human Connectome Project's raw imaging data and FreeSurfer outputs may be downloaded from https://db.humanconnectome.org.

## Code availability

The main standalone analysis Matlab code used in this study is available at https://doi.org/10.5281/zenodo.5912108. Additional non-standalone supporting code will be made available upon request.

## References

1. Geschwind N. Disconnexion syndromes in animals and man. Brain. 1965;88: 237–294.
2. Assaf Y, Johansen-Berg H, Thiebaut de Schotten M. The role of diffusion MRI in neuroscience. NMR Biomed. 2019;32: e3762. doi:https://doi.org/10.1002/nbm.3762
3. Aboitiz F, Scheibel AB, Fisher RS, Zaidel E. Fiber composition of the human corpus callosum. Brain Res. 1992;598: 143–153. doi:10.1016/0006-8993(92)90178-C
4. Zikopoulos B, Barbas H. Changes in prefrontal axons may disrupt the network in autism. J Neurosci. 2010;30: 14595–14609.
5. Zikopoulos B, García-Cabezas MÁ, Barbas H. Parallel trends in cortical gray and white matter architecture and connections in primates allow fine study of pathways in humans and reveal network disruptions in autism. PLoS Biol. 2018;16: e2004559.
6. Bullmore E, Sporns O. The economy of brain network organization. Nat Rev Neurosci. 2012;13: 336–349. doi:10.1038/nrn3214
7. Hofman MA. Evolution of the human brain: when bigger is better. Front Neuroanat. 2014;8: 15.
8. Markov NT, Ercsey-Ravasz M, Van Essen DC, Knoblauch K, Toroczkai Z, Kennedy H. Cortical high-density counterstream architectures. Science. 2013. pp. 1238406–1238406. doi:10.1126/science.1238406
9. Bassett DS, Bullmore ET. Small-world brain networks revisited. Neurosci. 2017;23: 499–516.
10. Buzsáki G, Mizuseki K. The log-dynamic brain: how skewed distributions affect network operations. Nat Rev Neurosci. 2014;15: 264–278. doi:10.1038/nrn3687

11. Rosen BQ, Halgren E. A Whole-Cortex Probabilistic Diffusion Tractography Connectome. eNeuro. 2021;8: ENEURO.0416-20.2020. doi:10.1523/ENEURO.0416-20.2020
12. Fischl B. FreeSurfer. Neuroimage. 2012;62: 774–781. doi:10.1016/j.neuroimage.2012.01.021
13. Donahue CJ, Sotiropoulos SN, Jbabdi S, Hernandez-Fernandez M, Behrens TE, Dyrby TB, et al. Using Diffusion Tractography to Predict Cortical Connection Strength and Distance: A Quantitative Comparison with Tracers in the Monkey. J Neurosci. 2016;36: 6758–6770. doi:10.1523/JNEUROSCI.0493-16.2016
14. van den Heuvel MP, de Reus MA, Feldman Barrett L, Scholtens LH, Coopmans FMT, Schmidt R, et al. Comparison of diffusion tractography and tract-tracing measures of connectivity strength in rhesus macaque connectome. Hum Brain Mapp. 2015;36: 3064–3075. doi:10.1002/hbm.22828
15. Arnatkeviciute A, Fulcher BD, Oldham S, Tiego J, Paquola C, Gerring Z, et al. Genetic influences on hub connectivity of the human connectome. Nat Commun. 2021;12: 4237. doi:10.1038/s41467-021-24306-2
16. Glasser MF, Coalson TS, Robinson EC, Hacker CD, Harwell J, Yacoub E, et al. A multi-modal parcellation of human cerebral cortex. Nature. 2016;536: 171–8. doi:10.1038/nature18933
17. Azevedo FAC, Carvalho LRB, Grinberg LT, Farfel JM, Ferretti REL, Leite REP, et al. Equal numbers of neuronal and nonneuronal cells make the human brain an isometrically scaled-up primate brain. J Comp Neurol. 2009;513: 532–541. doi:10.1002/cne.21974
18. DeFelipe J, Fariñas I. The pyramidal neuron of the cerebral cortex: Morphological and chemical characteristics of the synaptic inputs. Prog Neurobiol. 1992;39: 563–607. doi:10.1016/0301-0082(92)90015-7
19. Barbas H, Hilgetag CC, Saha S, Dermon CR, Suski JL. Parallel organization of contralateral and ipsilateral prefrontal cortical projections in the rhesus monkey. BMC Neurosci. 2005;6: 32. doi:10.1186/1471-2202-6-32
20. Schüz A, Braitenberg V. The human cortical white matter: quantitative aspects of cortico-cortical long-range connectivity. Cortical areas Unity Divers. 2002; 377–385.
21. Yeh F-C. Shape analysis of the human association pathways. Neuroimage. 2020;223: 117329. doi:https://doi.org/10.1016/j.neuroimage.2020.117329
22. Tremblay P, Dick AS. Broca and Wernicke are dead, or moving past the classic model of language neurobiology. Brain Lang. 2016;162: 60–71. doi:https://doi.org/10.1016/j.bandl.2016.08.004
23. Xuereb JH, Perry RH, Candy JM, Perry EK, Bonham JR. Nerve cell Loss in the thalamus in Alzheimer's disease and Parkinson's disease. Brain. 1991;114: 1363–1379.
24. Arcelli P, Frassoni C, Regondi MC, De Biasi S, Spreafico R. GABAergic neurons in mammalian thalamus: a marker of thalamic complexity? Brain Res Bull. 1997;42: 27–37.
25. Avino TA, Barger N, Vargas M V, Carlson EL, Amaral DG, Bauman MD, et al. Neuron numbers increase in the human amygdala from birth to adulthood, but not in autism. Proc Natl Acad Sci. 2018;115: 3710–3715.
26. Liewald D, Miller R, Logothetis N, Wagner HJ, Schüz A. Distribution of axon diameters in cortical white matter: an electron-microscopic study on three human brains and a macaque. Biol Cybern. 2014;108: 541–557. doi:10.1007/s00422-014-0626-2
27. Schüz A, Palm G. Density of neurons and synapses in the cerebral cortex of the mouse. J Comp Neurol. 1989;286: 442–455.
28. De Santis S, Drakesmith M, Bells S, Assaf Y, Jones DK. Why diffusion tensor MRI does well only some of the time: variance and covariance of white matter tissue microstructure attributes in the living human brain. Neuroimage. 2014;89: 35–44.
29. Huang SY, Tian Q, Fan Q, Witzel T, Wichtmann B, McNab JA, et al. High-gradient diffusion MRI reveals distinct estimates of axon diameter index within different white matter tracts in the in vivo human brain. Brain Struct Funct. 2020;225: 1277–1291. doi:10.1007/s00429-019-01961-2
30. Fan Q, Nummenmaa A, Witzel T, Ohringer N, Tian Q, Setsompop K, et al. Axon diameter index estimation independent of fiber orientation distribution using high-gradient diffusion MRI. Neuroimage. 2020;222: 117197.
31. Horowitz A, Barazany D, Tavor I, Bernstein M, Yovel G, Assaf Y. In vivo correlation between axon diameter and conduction velocity in the human brain. Brain Struct Funct. 2015;220: 1777–1788.
32. Tomasi S, Caminiti R, Innocenti GM. Areal differences in diameter and length of corticofugal projections. Cereb Cortex. 2012;22: 1463–1472.

33. Innocenti GM, Vercelli A, Caminiti R. The Diameter of Cortical Axons Depends Both on the Area of Origin and Target. Cereb Cortex. 2014;24: 2178–2188. doi:10.1093/cercor/bht070
34. Beaulieu C. The basis of anisotropic water diffusion in the nervous system – a technical review. NMR Biomed. 2002;15: 435–455. doi:https://doi.org/10.1002/nbm.782
35. Highley JR, Esiri MM, McDonald B, Roberts HC, Walker MA, Crow TJ. The size and fiber composition of the anterior commissure with respect to gender and schizophrenia. Biol Psychiatry. 1999;45: 1120–1127.
36. Schmahmann JD, Pandya DN. Cerebral White Matter — Historical Evolution of Facts and Notions Concerning the Organization of the Fiber Pathways of the Brain. J Hist Neurosci. 2007;16: 237–267. doi:10.1080/09647040500495896
37. Hagler DJ, Ahmadi ME, Kuperman J, Holland D, McDonald CR, Halgren E, et al. Automated white-matter tractography using a probabilistic diffusion tensor atlas: Application to temporal lobe epilepsy. Hum Brain Mapp. 2009;30: 1535–1547. doi:10.1002/hbm.20619
38. Spead O, Poulain FE. Trans-axonal signaling in neural circuit wiring. Int J Mol Sci. 2020;21: 5170.
39. Brysbaert M, Stevens M, Mandera P, Keuleers E. How Many Words Do We Know? Practical Estimates of Vocabulary Size Dependent on Word Definition, the Degree of Language Input and the Participant's Age . Frontiers in Psychology . 2016. p. 1116. Available: https://www.frontiersin.org/article/10.3389/fpsyg.2016.01116
40. Jin J, Maren S. Prefrontal-Hippocampal Interactions in Memory and Emotion . Frontiers in Systems Neuroscience . 2015. Available: https://www.frontiersin.org/article/10.3389/fnsys.2015.00170
41. Bazhenov M, Rulkov NF, Timofeev I. Effect of synaptic connectivity on long-range synchronization of fast cortical oscillations. J Neurophysiol. 2008;100: 1562–1575. doi:10.1152/jn.90613.2008
42. Vicente R, Gollo LL, Mirasso CR, Fischer I, Pipa G. Dynamical relaying can yield zero time lag neuronal synchrony despite long conduction delays. Proc Natl Acad Sci. 2008;105: 17157 LP – 17162. doi:10.1073/pnas.0809353105
43. Dickey CW, Verzhbinsky IA, Jiang X, Rosen BQ, Kajfez S, Stedelin B, et al. Widespread ripples synchronize human cortical activity during sleep, waking, and memory recall. bioRxiv. 2021; 2021.02.23.432582. doi:10.1101/2021.02.23.432582
44. Mak-McCully RA, Deiss SR, Rosen BQ, Jung KY, Sejnowski TJ, Bastuji H, et al. Synchronization of Isolated Downstates (K-Complexes) May Be Caused by Cortically-Induced Disruption of Thalamic Spindling. PLoS Comput Biol. 2014;10. doi:10.1371/journal.pcbi.1003855
45. Beul SF, Barbas H, Hilgetag CC. A Predictive Structural Model of the Primate Connectome. Sci Rep. 2017;7: 1–12. doi:10.1038/srep43176
46. Deco G, Sanz Perl Y, Vuust P, Tagliazucchi E, Kennedy H, Kringelbach ML. Rare long-range cortical connections enhance human information processing. Curr Biol. 2021;31: 4436-4448.e5. doi:https://doi.org/10.1016/j.cub.2021.07.064
47. Aboitiz F, López J, Montiel J. Long distance communication in the human brain: timing constraints for inter-hemispheric synchrony and the origin of brain lateralization. Biol Res. 2003;36: 89–99.
48. Peters A, Payne BR, Budd J. A numerical analysis of the geniculocortical input to striate cortex in the monkey. Cereb Cortex. 1994;4: 215–229.
49. Chung S, Ferster D. Strength and orientation tuning of the thalamic input to simple cells revealed by electrically evoked cortical suppression. Neuron. 1998;20: 1177–1189.
50. Van Den Heuvel MP, Sporns O. Rich-club organization of the human connectome. J Neurosci. 2011;31: 15775–15786.
51. Van Essen DC, Smith SM, Barch DM, Behrens TEJ, Yacoub E, Ugurbil K. The WU-Minn Human Connectome Project: An overview. Neuroimage. 2013;80: 62–79. doi:10.1016/j.neuroimage.2013.05.041
52. Behrens TEJ, Berg HJ, Jbabdi S, Rushworth MFS, Woolrich MW. Probabilistic diffusion tractography with multiple fibre orientations: What can we gain? Neuroimage. 2007;34: 144–155. doi:10.1016/j.neuroimage.2006.09.018
53. Jenkinson M, Beckmann CF, Behrens TEJ, Woolrich MW, Smith SM. FSL. Neuroimage. 2012;62: 782–790. doi:10.1016/j.neuroimage.2011.09.015
54. Tournier JD, Smith R, Raffelt D, Tabbara R, Dhollander T, Pietsch M, et al. MRtrix3: A fast, flexible and open software framework for medical image processing and visualisation. Neuroimage. 2019;202: 116137.

doi:10.1016/j.neuroimage.2019.116137
55. Tournier JD, Calamante F, Connelly A. Improved probabilistic streamlines tractography by 2nd order integration over fibre orientation distributions. Proceedings of the international society for magnetic resonance in medicine. John Wiley & Sons, Inc. New Jersey, USA; 2010.
56. Meyer M, Desbrun M, Schröder P, Barr AH. Discrete Differential-Geometry Operators for Triangulated 2-Manifolds. 2003. pp. 35–57. doi:10.1007/978-3-662-05105-4_2
57. Wegiel J, Flory M, Kaczmarski W, Brown WT, Chadman K, Wisniewski T, et al. Partial Agenesis and Hypoplasia of the Corpus Callosum in Idiopathic Autism. J Neuropathol Exp Neurol. 2017;76: 225–237. doi:10.1093/jnen/nlx003
58. Williams EJ. The comparison of regression variables. J R Stat Soc Ser B. 1959;21: 396–399.
59. Ji JL, Spronk M, Kulkarni K, Repovš G, Anticevic A, Cole MW. Mapping the human brain's cortical-subcortical functional network organization. Neuroimage. 2019;185: 35–57. doi:10.1016/j.neuroimage.2018.10.006
60. Blinkov SM, Glezer II. The human brain in figures and tables: a quantitative handbook. Basic Books; 1968.
61. von Bartheld CS, Bahney J, Herculano-Houzel S. The search for true numbers of neurons and glial cells in the human brain: A review of 150 years of cell counting. J Comp Neurol. 2016;524: 3865–3895. doi:10.1002/cne.24040
62. Beckmann H, Lauer M. The human striatum in schizophrenia. II. Increased number of striatal neurons in schizophrenics. Psychiatry Res Neuroimaging. 1997;68: 99–109.
63. Baker KG, Halliday GM, Hornung J-P, Geffen LB, Cotton RGH. Distribution, morphology and number of monoamine-synthesizing and substance P-containing neurons in the human dorsal raphe nucleus. Neuroscience. 1991;42: 757–775.
64. Mouton PR, Pakkenberg B, Gundersen HJG, Price DL. Absolute number and size of pigmented locus coeruleus neurons in young and aged individuals. J Chem Neuroanat. 1994;7: 185–190.
65. Eriksen N, Stark AK, Pakkenberg B. Age and Parkinson's disease-related neuronal death in the substantia nigra pars compacta. Birth, life death dopaminergic neurons Subst Nigra. 2009; 203–213.
66. Mufson EJ, Ginsberg SD, Ikonomovic MD, DeKosky ST. Human cholinergic basal forebrain: chemoanatomy and neurologic dysfunction. J Chem Neuroanat. 2003;26: 233–242.
67. Rivara C, Sherwood CC, Bouras C, Hof PR. Stereologic characterization and spatial distribution patterns of Betz cells in the human primary motor cortex. Anat Rec Part A Discov Mol Cell Evol Biol An Off Publ Am Assoc Anat. 2003;270: 137–151.
68. Wada A, Goto J, Goto N, Kawamura N, Matsumoto K. Are There One Million Nerve Fibres in the Human Medullary Pyramid? Okajimas Folia Anat Jpn. 2001;77: 221–224. doi:10.2535/ofaj1936.77.6_221

## S1 Appendix: Extended Methods and Results

### Diffusion MRI

The diffusion-weighted MRI (dMRI) connectivity data used to estimate inter-parcel axon totals was described in our prior report [1] whose data are available in full at https://doi.org/10.5281/zenodo.4060485. Preprocessed imaging data for 1,065 healthy young adults were retrieved from the Human Connectome Project WU-Minn consortium 1200 release [2] (https://db.humanconnectome.org). We segmented the cortex into 180 parcels per hemisphere following the HCP-MMP1.0 atlas [3] and performed probabilistic tractography using the probtrackX tool [4] from FSL [5] using tractography parameters detailed in our prior report [1]. This analysis yielded a 360 x 360 dMRI connectivity matrix for each subject which provided the example data for applying the method presented here. For probtrackX-derived connectivity, the raw unit of dMRI connectivity strength is the number of streamlines connecting seed and target regions. The absolute magnitude of this metric is arbitrary as it scales with the number of samples drawn from the probability distribution of diffusion parameters in each voxel, in our analysis 5,000.

The individual pairwise streamline counts and fiber tract length matrices for the replication analysis were described in [6] whose data are available at https://doi.org/10.5281/zenodo.4733297. These data consist of a 972 subject subset of the 1,065 WU-Minn HCP subjects included in our primary analysis. Arnatkeviciute and colleagues similarly segmented the cortex following the HCP-MMP1.0 atlas [3]. In contrast to our primary dataset, tractography was performed with MRtrix3 [7] using second-order integration over fiber orientation distributions (iFOD2) [8], see [6] for details. When confined to the same subject subset and non-null connections, the pairwise tract lengths and log-transformed streamline counts are highly correlated ($r^2 = 0.78$ and $r^2 = 0.69$, respectively) between Arnatkeviciute et al. [6] and our study [1]. The rate of exponential decay in the number of streamlines vs fiber tract distance is also similar, $\lambda = 26.1$ mm in their study vs 23.4 mm in ours, though less connectivity variance

601 is explained by distance in their results ($r^2$ = 0.12 vs. $r^2$ = 0.52). Results for these tractography data are

602 shown in S2 Fig.

603

604 Cross-sectional area of the corpus callosum, white matter volume, and parcel areas

605 The HCP WU-Minn consortium 1200 release [2] includes the standard outputs from the FreeSurfer

606 `recon-all` pipeline [9]. With default parameters, this pipeline labels the 1 $mm^3$ voxels of the `aseg.mgz`

607 volume which contain the corpus callosum with a fixed 5mm lateral extent. Dividing the number of

608 callosum-label voxels by 5 yields an estimate of its cross-sectional area, in $mm^2$. The total white matter

609 volume is reported in the `aseg.stats` output of `mri_segstats`. Parcel areas and adjacency were

610 determined [10] on triangular mesh of each subject's reconstruct white matter surface, or white matter

611 – gray matter interface (`?h.white`). These data were used for both the primary and replication analyses.

612

613 Cross-sectional fiber packing density in corpus callosum and other hemispheric white

614 matter

615 Our estimate of callosal fiber density was based on the electron microscopy (EM) study by Aboitiz and

616 colleagues [11] who reported a fiber density of 38 per 100 $\mu m^2$ or $3.7 \times 10^5$ axons/$mm^2$ after accounting

617 for tissue shrinkage to 96% volume after Epon fixation [12]. This is consistent with their finding of

618 $2.65 \times 10^5$ axons/$mm^2$ as measured with light-microscopy in twenty brains as well, assuming shrinkage

619 to 43% volume for paraffin fixation [12] and an estimated ~20% of fibers not detectable with light

620 microscopy [11], as well as the $2.83 \times 10^5$ non-exhaustively counted axons per $mm^2$ reported in a more

621 recent EM study of callosal axon diameter in two brains [13]. This value was derived by dividing the

622 reported mean count of axons per callosal region by the callosal area surveyed, and correcting for EM

623 preparation tissue shrinkage. An additional light microscopy study of callosal axon density in eleven

624 control cortices reports an average of $1.12 \times 10^5$ myelinated axons per $mm^2$ [14], assuming shrinkage to

625 shrinkage to 43% volume. This somewhat lower figure may be explained by the inclusion of four

children's cortices in their cohort, or by mis-assumed shrinkage, but all reports are within half an order-of-magnitude of each other.

## Distance matched intra- vs. inter-hemispheric dMRI connectivity

One assumption of the method described in this report is that the dMRI tractography methodology has approximately similar sensitivity to callosal and ipsilateral connections. This is difficult to determine without ground truth connectivity, as intra- and inter-hemispheric connections may have true anatomical differences. Nevertheless, we examined distance-matched intra- vs inter-hemispheric connections (Fig 1*C*) and found no statistical evidence that they are different. Pairwise connections were averaged in 15 distance bins, log-transformed and linear fits obtained for intra- and inter-hemispheric connections. For the overlapping distance domain, the intra-hemispheric slope is -0.30, 95% confidence interval = [-0.33 -0.26] with an intercept of 6.18 [5.91 6.45] and the inter-hemispheric slope is -0.26 [-0.29 -0.24] and intercept of 5.93 [5.72 6.14]; the 95% confidence intervals of both parameters are overlapping. In addition, a paired r-test of correlation differences [15] failed to reject the null hypothesis, $p = 0.58$. The parity between distance-matched intra- and inter-hemispheric connections also holds when the linear fit is obtained for over the entire distance domain, with an intra-hemispheric slope and intercept -.31 [-0.33 -0.28] and 6.24 [6.01 6.46], respectively; -.28 [-0.30 -0.25] and 6.00 [5.78 6.23] for inter-hemispheric connections. In the replication analysis with alternative tractography data [6] (S2 Fig C) the paired r-test likewise failed to reject the null hypothesis, $p = 0.34$. The intra-hemispheric slope and intercept are -.37 [-0.37 -0.78] and 4.19 [3.25 5.13], respectively; -.25 [-0.30 -0.20] and 3.30 [2.82 3.79] for inter-hemispheric connections.

## Estimating axon counts and axon volume from dMRI

From the histological estimate of callosal fiber density, MRI-derived measures of callosal cross-sectional area and white matter connectivity, the conversion factor between dMRI connectivity and physical axons can be estimated as follows:

Eq. 1.1 $N_{callosum} = A_{callosum} * D_{callosum}$

Eq. 1.2 $C_{axon} = \frac{Ncallosum}{M_{dMRI}}$

Where $A_{callosum}$ is the cross-sectional area (mm$^2$), $D_{callosum}$ is the assumed fiber density (3.7x10$^5$ axons/mm$^2$) of the corpus callosum, $N_{callosum}$ is the estimated total number of callosal fibers, $M_{dMRI}$ is the magnitude of dMRI callosal connectivity, in our case, the number of tractography streamlines, and $C_{axon}$ is the conversion factor from dMRI to physical fibers (axons/streamline).

In addition to connectivity strength, or number of streamlines, the dMRI tractography analysis also yields a mean streamline length for every parcel-pair connection. After converting dMRI connectivity strength to physical axon count as described above, the total volume of the estimated axons can be calculated as follows:

Eq. 2.1 $WM_{volume} = \sum_{i=1}^{N_{pair}} l_i * n_i * C_{axon} * \frac{1}{D_{callosum}}$

Eq. 2.2 $WM_{volume} = \sum_{i=1}^{N_{pair}} l_i * n_i * \frac{A_{callosum}}{M_{dMRI}}$

Where $WM_{volume}$ is the estimated axonal white matter volume (mm$^3$) and $N_{pair}$ is the total number of parcel pairs. $l_i$ and $n_i$ are the length (mm) and number of dMRI streamlines in the $i^{th}$ parcel pair. Eq. 2.1 can be simplified into Eq. 2.2 by substituting Eqs. 1.1 and 1.2 into 2.1.

## Parcel grouping into functional networks

The parcel ordering and the ten functional networks shown in Fig 1*A* were defined in our previous report [1] and were modified from twelve networks identified by Ji and colleagues in a resting-state fMRI study on the HCP cohort [16] by merging the primary and secondary visual networks as well as the ventral and posterior multimodal networks.

676 Effects of sex and age on inter-hemispheric connectivity

677 In their histological study of 20 cortices , Aboitiz and colleagues [11] found no significant effects of sex
678 or age on the total number of fibers, fiber density, and cross-sectional area of the corpus callosum. As
679 we assume a constant fiber density, our estimate of the total number of inter-hemispheric fibers is a
680 linear function of the callosal cross-sectional area. As the ages of the HCP 1200 cohort are grouped
681 into four broad ranges in the open access data, we investigated the effects of sex and age on the
682 estimated number inter-hemispheric axons with 2x4 fixed effects ANOVA, treating the age group
683 factor as categorical. Mean and individual values are shown in S3 Fig. Note that while the number of
684 pairwise axons is approximately log-normally distributed across areal pairs, it is approximately
685 normally distributed across individuals.

686 We found that, on average, males have $2.61 \times 10^8$ inter-hemispheric axons, 95% confidence interval
687 = [$2.58 \times 10^8$ $2.64 \times 10^8$] and females have $2.50 \times 10^8$ [$2.47 \times 10^8$ $2.52 \times 10^8$] axons. Subjects ages 22-25, 26-
688 30, 31-35, and 36+ year old have $2.50 \times 10^8$ [$2.46 \times 10^8$ $2.55 \times 10^8$], $2.58 \times 10^8$ [$2.55 \times 10^8$ $2.61 \times 10^8$], $2.55 \times 10^8$
689 [$2.51 \times 10^8$ $2.59 \times 10^8$], and $2.35 \times 10^8$ [$2.15 \times 10^8$ $2.54 \times 10^8$] axons, respectively. Intervals show
690 bootstrapped 95% confidence. We find no effect of sex on the number of inter-hemispheric axons,
691 $F_{1,1064} = 3.471$, $p = 0.0627$. Removing the one female outlier does not bring the mean difference into
692 statistical significance, $F_{1,1063} = 3.653$, $p = 0.0562$. The interaction of sex and age on the number of
693 inter-hemispheric axons is likewise not significant $F_{3,1064} = 2.282$, $p = 0.0776$. Age does significantly
694 affect the number of inter-hemispheric neurons, $F_{3,1064} = 5.100$, $p = 0.0017$. Post-hoc pairwise tests
695 show that only the difference between the 22-25 and 26-30 year old age groups is significant, $F_{1,1064}$ =
696 7.646, $p = 0.0058$. These results are broadly consistent with those of Aboitiz et al. [11]. A more in-
697 depth examination of the effects of age on corpus callosum requires a cohort with which includes
698 more older subjects as well as more precise age values.

699

700 Thalamo-cortical fiber volume estimation

701 The scope of our previous dMRI tractography study [1] was confined to cortico-cortical (including
702 cortico-hippocampal) connectivity. In order to estimate the total volume of thalamo-cortical axons, we
703 first calculated the number of excitatory thalamic neurons by summing the total number of neurons in
704 the thalamus [17], excluding the reticular nucleus, zona incerta, limitans/suprageniculate, and
705 subthalamus, and including from the remainder the ~62% proportion of thalamic neurons that are
706 excitatory [18]. The number of such neurons is $22.6 \times 10^6$. We assumed that each such thalamic neuron
707 projects a single axon to the cortex, and we allocated these axons to cortical parcels in proportion to
708 their area. The inverse callosal packing density was used for effective cross-sectional area, as with
709 cortico-cortical connections. To estimate the length of thalamo-cortical fiber tracts, for each parcel $i$,
710 we first identified the thalamic voxel nearest to parcel's centroid. We then used the inter-parcel fiber
711 tract length [1] from the centroid of parcel $i$ to the identified parathalamic parcel centroid. To this
712 figure we added the Euclidean distance from the parathalamic centroid to the nearest voxel of the
713 thalamus, ensuring that estimated thalamo-cortical fiber tract length is always non-zero. As with
714 cortico-cortical connections, the total white matter volume of each connection was estimated by taking
715 the product of the number of axons, the effective cross-sectional area, and the estimated fiber tract
716 length (Eq. 2).

717

718 Estimation of proportion of actual inter-areal axons to the number that would be
719 needed for complete inter-connectivity

720 We estimated that the total number of inter-areal axons is ~$2.43 \times 10^9$. Assuming $n = 16.34 \times 10^9$ total
721 cortical neurons (including interneurons) [19] , the total number of connections needed for complete
722 whole-cortex connectivity is $n(n-1) = 2.67 \times 10^{20}$. We estimated the neural density of the cortex as
723 ~92,300 neurons/mm$^2$ by dividing $16.34 \times 10^9$ by $1.77 \times 10^5$ mm$^2$ mean white–gray surface area of the

724 HCP cohort used. The total number of connections needed for complete inter-connectivity within each

725 area is approximately $1.18 \times 10^{18}$, given by

726

727 Eq. 3.1 $N_{completeIntra-areal} = \sum_{i=1}^{N_{parcel}} \left(A_{parcel} * D_{neuron}\right)^2$

728

729 Where $A_{parcel}$ is the area of each parcel and $D_{neuron}$ the neural density. Subtracting the connections

730 needed for within-area inter-connectivity from whole cortex interconnectivity yields $2.66 \times 10^{20}$, which is

731 $1.10 \times 10^{11}$ times greater than the number of inter-areal contacts we calculate with our method.

732

733 Number of neurons in non-cortical regions communicating with the cortex

734 The number of neurons in different human brain regions has been reviewed by Blinkov and Glexer [21]

735 and von Bartheld et al. [22]. The number of neurons in the amygdala have been estimated as ~$13 \times 10^6$

736 [23], striatum as ~$55 \times 10^6$ [24], and thalamus as ~$23 \times 10^6$ (thalamocortical, see above). These are the

737 only recipients or targets of cortical connections with significant numbers of neurons. Other locations,

738 such those which are the origins of serotonin [25], norepinephrine [26], dopamine [27], or

739 acetylcholine [28] afferents to the cortex all have ~50,000 axons each. Summed together, the number

740 of cells in all of the above structures comes to ~0.5% of the number of cortical cells. Direct projections

741 outside of the brain are exceedingly rare, with the number of Betz cells in the primary motor cortex

742 [29] or medullary pyramid [30] both estimated as ~100,000. It is difficult to escape the conclusion that,

743 at least in humans, the cortex communicates mainly with itself.

744

745

746 References


747 1. Rosen BQ, Halgren E. A Whole-Cortex Probabilistic Diffusion Tractography Connectome. eNeuro. 2021;8:
748 ENEURO.0416-20.2020. doi:10.1523/ENEURO.0416-20.2020
749 2. Van Essen DC, Smith SM, Barch DM, Behrens TEJ, Yacoub E, Ugurbil K. The WU-Minn Human
750 Connectome Project: An overview. Neuroimage. 2013;80: 62–79. doi:10.1016/j.neuroimage.2013.05.041
751 3. Glasser MF, Coalson TS, Robinson EC, Hacker CD, Harwell J, Yacoub E, et al. A multi-modal parcellation of
752 human cerebral cortex. Nature. 2016;536: 171–8. doi:10.1038/nature18933

4. Behrens TEJ, Berg HJ, Jbabdi S, Rushworth MFS, Woolrich MW. Probabilistic diffusion tractography with multiple fibre orientations: What can we gain? Neuroimage. 2007;34: 144–155. doi:10.1016/j.neuroimage.2006.09.018
5. Jenkinson M, Beckmann CF, Behrens TEJ, Woolrich MW, Smith SM. FSL. Neuroimage. 2012;62: 782–790. doi:10.1016/j.neuroimage.2011.09.015
6. Arnatkeviciute A, Fulcher BD, Oldham S, Tiego J, Paquola C, Gerring Z, et al. Genetic influences on hub connectivity of the human connectome. Nat Commun. 2021;12: 4237. doi:10.1038/s41467-021-24306-2
7. Tournier JD, Smith R, Raffelt D, Tabbara R, Dhollander T, Pietsch M, et al. MRtrix3: A fast, flexible and open software framework for medical image processing and visualisation. Neuroimage. 2019;202: 116137. doi:10.1016/j.neuroimage.2019.116137
8. Tournier JD, Calamante F, Connelly A. Improved probabilistic streamlines tractography by 2nd order integration over fibre orientation distributions. Proceedings of the international society for magnetic resonance in medicine. John Wiley & Sons, Inc. New Jersey, USA; 2010.
9. Fischl B. FreeSurfer. Neuroimage. 2012;62: 774–781. doi:10.1016/j.neuroimage.2012.01.021
10. Meyer M, Desbrun M, Schröder P, Barr AH. Discrete Differential-Geometry Operators for Triangulated 2-Manifolds. 2003. pp. 35–57. doi:10.1007/978-3-662-05105-4_2
11. Aboitiz F, Scheibel AB, Fisher RS, Zaidel E. Fiber composition of the human corpus callosum. Brain Res. 1992;598: 143–153. doi:10.1016/0006-8993(92)90178-C
12. Schüz A, Palm G. Density of neurons and synapses in the cerebral cortex of the mouse. J Comp Neurol. 1989;286: 442–455.
13. Liewald D, Miller R, Logothetis N, Wagner HJ, Schüz A. Distribution of axon diameters in cortical white matter: an electron-microscopic study on three human brains and a macaque. Biol Cybern. 2014;108: 541–557. doi:10.1007/s00422-014-0626-2
14. Wegiel J, Flory M, Kaczmarski W, Brown WT, Chadman K, Wisniewski T, et al. Partial Agenesis and Hypoplasia of the Corpus Callosum in Idiopathic Autism. J Neuropathol Exp Neurol. 2017;76: 225–237. doi:10.1093/jnen/nlx003
15. Williams EJ. The comparison of regression variables. J R Stat Soc Ser B. 1959;21: 396–399.
16. Ji JL, Spronk M, Kulkarni K, Repovš G, Anticevic A, Cole MW. Mapping the human brain's cortical-subcortical functional network organization. Neuroimage. 2019;185: 35–57. doi:10.1016/j.neuroimage.2018.10.006
17. Xuereb JH, Perry RH, Candy JM, Perry EK, Bonham JR. Nerve cell Loss in the thalamus in Alzheimer's disease and Parkinson's disease. Brain. 1991;114: 1363–1379.
18. Arcelli P, Frassoni C, Regondi MC, De Biasi S, Spreafico R. GABAergic neurons in mammalian thalamus: a marker of thalamic complexity? Brain Res Bull. 1997;42: 27–37.
19. Azevedo FAC, Carvalho LRB, Grinberg LT, Farfel JM, Ferretti REL, Leite REP, et al. Equal numbers of neuronal and nonneuronal cells make the human brain an isometrically scaled-up primate brain. J Comp Neurol. 2009;513: 532–541. doi:10.1002/cne.21974
20. DeFelipe J, Fariñas I. The pyramidal neuron of the cerebral cortex: Morphological and chemical characteristics of the synaptic inputs. Prog Neurobiol. 1992;39: 563–607. doi:10.1016/0301-0082(92)90015-7
21. Blinkov SM, Glezer II. The human brain in figures and tables: a quantitative handbook. Basic Books; 1968.
22. von Bartheld CS, Bahney J, Herculano-Houzel S. The search for true numbers of neurons and glial cells in the human brain: A review of 150 years of cell counting. J Comp Neurol. 2016;524: 3865–3895. doi:10.1002/cne.24040
23. Avino TA, Barger N, Vargas M V, Carlson EL, Amaral DG, Bauman MD, et al. Neuron numbers increase in the human amygdala from birth to adulthood, but not in autism. Proc Natl Acad Sci. 2018;115: 3710–3715.
24. Beckmann H, Lauer M. The human striatum in schizophrenia. II. Increased number of striatal neurons in schizophrenics. Psychiatry Res Neuroimaging. 1997;68: 99–109.
25. Baker KG, Halliday GM, Hornung J-P, Geffen LB, Cotton RGH. Distribution, morphology and number of monoamine-synthesizing and substance P-containing neurons in the human dorsal raphe nucleus. Neuroscience. 1991;42: 757–775.
26. Mouton PR, Pakkenberg B, Gundersen HJG, Price DL. Absolute number and size of pigmented locus

805 coeruleus neurons in young and aged individuals. J Chem Neuroanat. 1994;7: 185–190.
806 27. Eriksen N, Stark AK, Pakkenberg B. Age and Parkinson's disease-related neuronal death in the substantia
807 nigra pars compacta. Birth, life death dopaminergic neurons Subst Nigra. 2009; 203–213.
808 28. Mufson EJ, Ginsberg SD, Ikonomovic MD, DeKosky ST. Human cholinergic basal forebrain:
809 chemoanatomy and neurologic dysfunction. J Chem Neuroanat. 2003;26: 233–242.
810 29. Rivara C, Sherwood CC, Bouras C, Hof PR. Stereologic characterization and spatial distribution patterns of
811 Betz cells in the human primary motor cortex. Anat Rec Part A Discov Mol Cell Evol Biol An Off Publ Am
812 Assoc Anat. 2003;270: 137–151.
813 30. Wada A, Goto J, Goto N, Kawamura N, Matsumoto K. Are There One Million Nerve Fibres in the Human
814 Medullary Pyramid? Okajimas Folia Anat Jpn. 2001;77: 221–224. doi:10.2535/ofaj1936.77.6_221
815

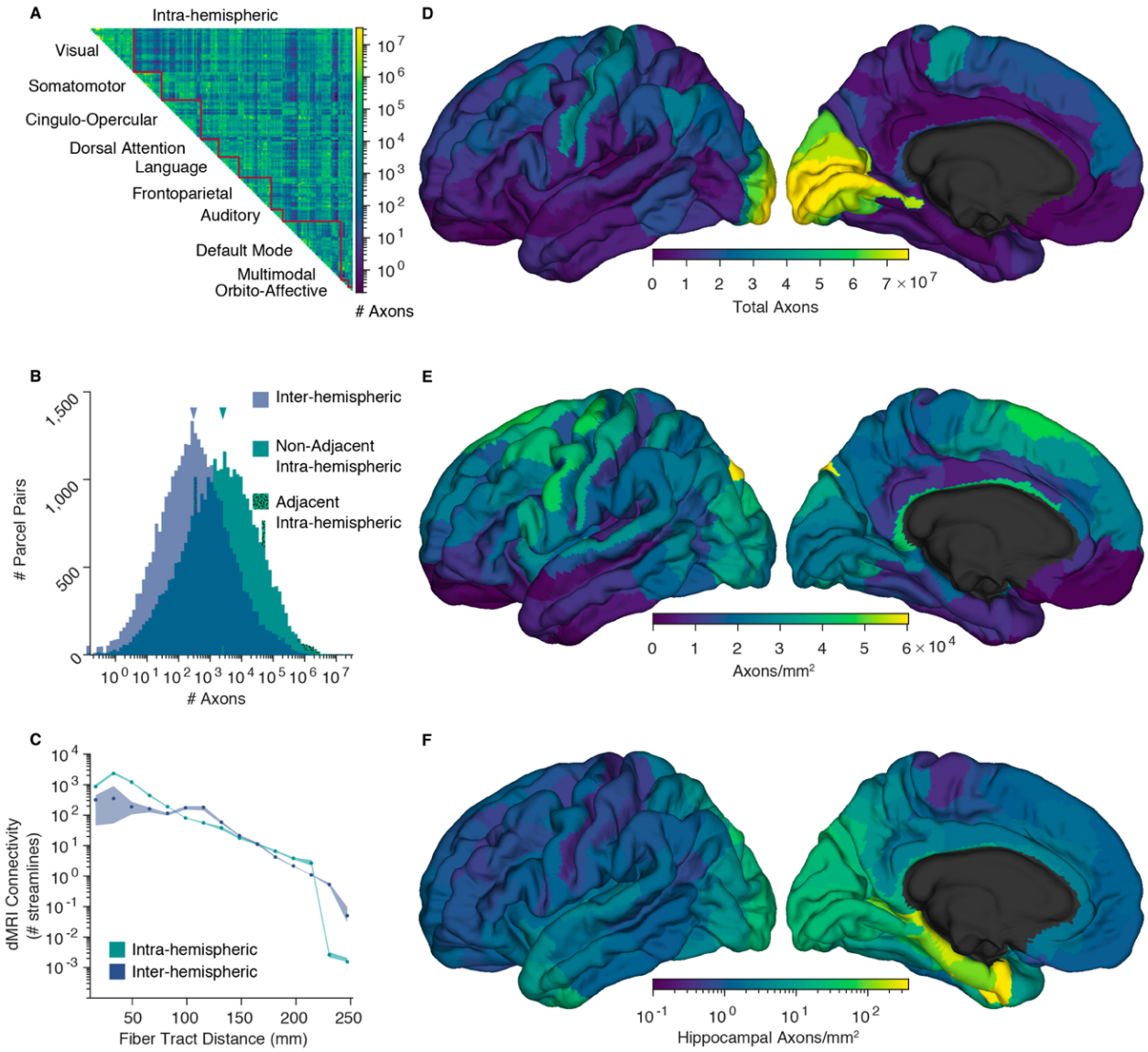


**S2 Fig: Replication results.** Results obtained by repeating the analysis using an alternative tractography dataset [1] (A) Connectivity matrix of intra-hemispheric axon counts, averaged across the two hemispheres. Parcels are ordered into 10 functional networks. (B) Histograms showing the distribution of inter- and intra-hemispheric pairwise axon counts. Physically adjacent and non-adjacent parcel pair intra-hemispheric histograms are stacked. Median connectivity, shown in gray, is ~2,500 axons between cortical areas in the same hemisphere, and ~300 inter-hemispherically. Parcel pairs with zero axons connecting them are represented by the bars left of the y-axis. (C) dMRI connectivity as

a function fiber tract distance. Pairwise values averaged within 15 fiber-length bins. Shading shows bootstrapped 95% confidence intervals. (D-F) axons counts and densities averaged across the two hemispheres and visualized on the left fsaverage template cortex [2]. (D) total axons connecting each parcel to all others. (E) axons connecting each parcel to all others, normalized by the reference parcel's area. (F) axons connecting the hippocampus to the rest of the cortex, normalized by the area of the cortical parcel, shown in log scale.


1. Arnatkeviciute A, Fulcher BD, Oldham S, Tiego J, Paquola C, Gerring Z, et al. Genetic influences on hub connectivity of the human connectome. Nat Commun. 2021;12: 4237. doi:10.1038/s41467-021-24306-2
2. Fischl B. FreeSurfer. Neuroimage. 2012;62: 774–781. doi:10.1016/j.neuroimage.2012.01.02


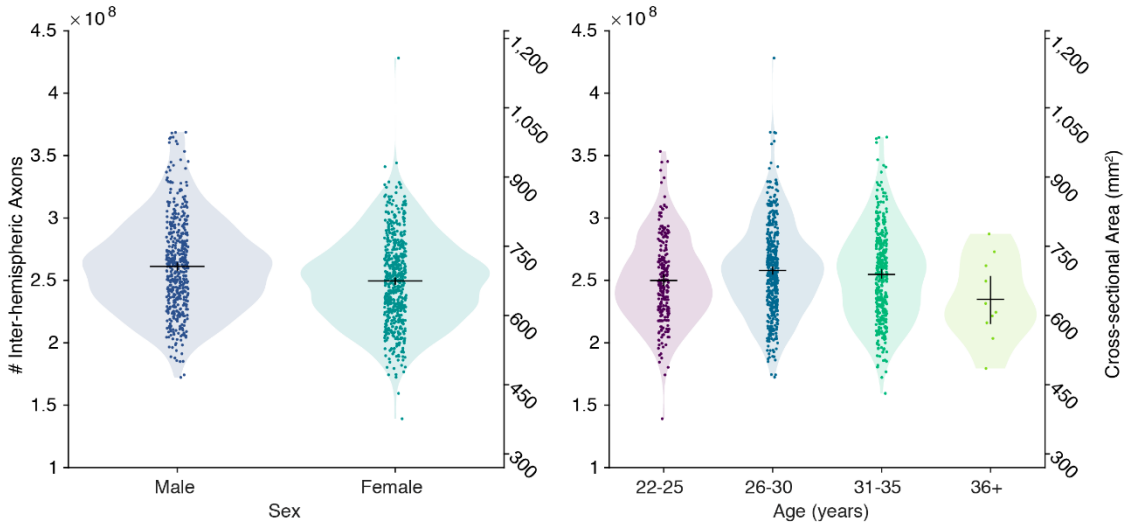


**S3 Fig: Effects of sex and age on the inter-hemispheric connectivity.** Each individual's total number of estimated inter-hemispheric axons is shown with a marker. The black horizonal bars show the group means and vertical bars the bootstrapped 95% confidence intervals these means. Shading shows a kernel density estimate of the group distributions. Note that while the number of pairwise axons is approximately log-normally distributed across areal pairs, it is approximately normally

distributed across individuals. The only significant group difference is between the 22-15 and 25-30 age groups, $F_{1,1064} = 7.646$, $p = 0.0058$. Interactions between sex and age effect were not significant. As we assume a constant fiber density, our estimate the total number of inter-hemispheric fibers is a linear multiple of the callosal cross-sectional area.

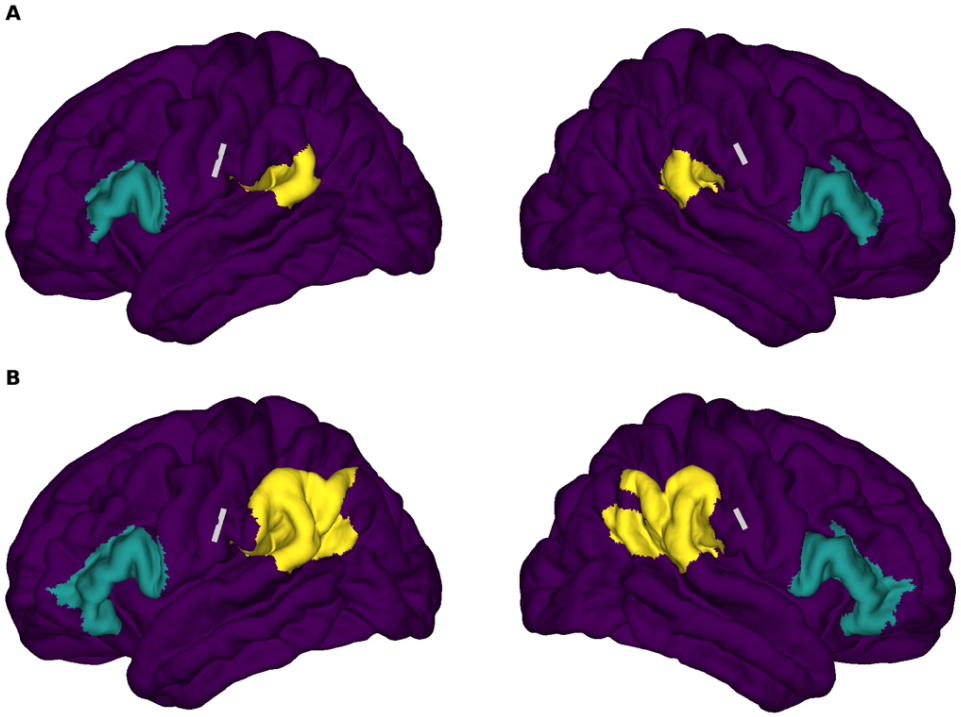


**S4 Fig: Arcuate / superior lateral fasciculus termination fields.** In order to estimate the fraction of tract axons that travel the entire length of the tract, it's termination fields, centered on Broca's and Wernicke's areas, were manually defined in terms of HCP-MMP1.0 parcels according to consensus definitions [1]. (A) Conservative definitions where the anterior termination field, in teal, is composed of parcels 44, 45, 6r, IFSa, IFSp, and FOP4 and the posterior termination field, in yellow, is composed of parcels PSL, RI, STV, and PFcm. For this definition trans-terminal axons account for 0.6% and 0.8% of tract axons in the left and right hemispheres. (B) Liberal definitions in which parcels 47l and p47r were added anteriorly and parcels PF, PFm, and PGi were added posteriorly, resulting in trans-terminal

axons accounting for 1.9% and 2.9% of tract axons in the left and right hemispheres. Gray lines indicate the approximate locations at which the tract diameter, used to estimate the total number of tract axons were ascertained [2].


1. Tremblay P, Dick AS. Broca and Wernicke are dead, or moving past the classic model of language neurobiology. Brain Lang. 2016;162: 60–71. doi:https://doi.org/10.1016/j.bandl.2016.08.004
2. Yeh F-C. Shape analysis of the human association pathways. Neuroimage. 2020;223: 117329. doi:https://doi.org/10.1016/j.neuroimage.2020.117329


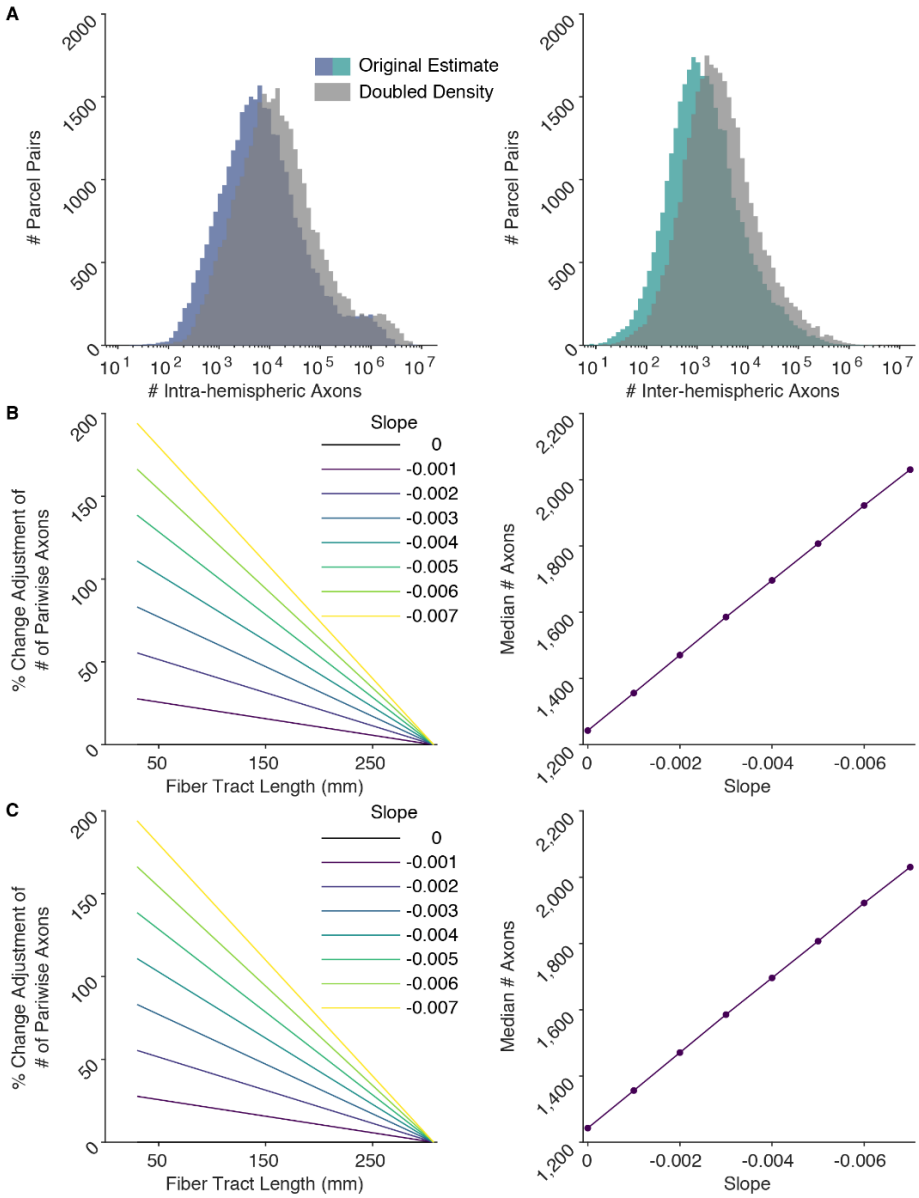

869 **S5 Fig: Simulated effect of short axon underestimation on pairwise axon counts.** In order to
870 explore the possibility that dMRI tractography is less sensitive to shorter connections the streamline-to-
871 axon ratio was increased linearly with inverse fiber length using a range of slope parameters. Packing
872 density was assumed to be reciprocally decreased in order to fix a constant total cerebral white matter
873 volume. (A) Distributions of Intra- and inter-hemispheric inter-areal axons counts. Gray histograms
874 show the effect of uniformly halfling the ratio and doubling the assumed packing density. (B) intra-
875 hemispheric and (C) inter-hemispheric adjustments to the # of pairwise axons as a function of inverse
876 fiber tract length and the resultant increase in median axon count as a function of the adjustments'
877 slope parameter. At slope = 0, values are unadjusted from the primary analysis. Large adjustments
878 only increase median counts modestly in the context of the log-normal distribution. For example, for
879 intra-hemispheric connections (B), at a slope of 0.004, the number of the shortest axons is about
880 doubled (i.e., corresponding to doubling the axon density and halving the sensitivity of dMRI to
881 axons), but the median number of inter-parcel axons only increases by ~36%.